Progress In Electromagnetics Research, Vol. 149, 281–289, 2014

Realizing Flexible Ultra-Flat-Band Slow Light in Hybrid Photonic Crystal Waveguides for Efficient Out-of-Plane Coupling

Jianhao Zhang[1], Yaocheng Shi[1, *], and Sailing He[1, 2]

Abstract—The realization of slow light with ultra-flat dispersion in hybrid photonic crystal (HPhC) waveguide is systematically investigated. Metal strips have been introduced to the photonic crystal (PhC) waveguide. The dispersion of the odd mode is commendably flattened in the leaky region. Ultra-flat-band slow light with nearly constant average group indices of 192 over 2 nm (i.e., 330 GHz) bandwidth is achieved. Flexible tuning for the ultra-high group index can also be achieved while keeping the normalized delay-bandwidth product fairly high. The introduction of the metal strips is further demonstrated to help reduce the azimuthal angle of the far field and provide a high coupling efficiency.

1. INTRODUCTION

Cavity-free slow light has attracted increasing interest, particularly for cavity-free, low-threshold and even threshold-free nanolasing [1]. In addition to dielectric structures for slow light, a large Purcell factor can also be obtained in plasmonic slow-light heterostructures for special cases according to cavity quantum electrodynamics (CQED), where the group velocity of the plasmons is close to zero. Low-threshold operation can be achieved since spontaneous emission can be efficiently channeled into the stopped-light mode [2–4]. However, slow-light for lasing applications always operates in the guided mode region and thus has a low out-coupling efficiency. Dragging the slow mode from the guided mode region to the leaky region may help improve the emission efficiency. On the other hand, only a small portion of light whose wave vector is near the slow point (usually, the zero point or Bloch point) can achieve a sufficient slow-light effect. A flattened dispersion, which results in a widened band of wave vectors for the same frequency can predictably enhance the Purcell effect [5–7] by slowing down a greater portion of light. For this reason, it is desirable to obtain flat-band slow light in the leaky region with small dispersion (for the applications of enhanced out-of-plane coupling of amplified spontaneous emission), or stopped-light mode at a certain frequency (for the applications of monochromatic lasing) with an ultra-high group index.

When it comes to directive light emission from a waveguide, cavity or homogeneous gain material, efficient light coupling between the free space and a state of confinement, particularly the slow mode, is difficult to realize. Distributed Bragg reflectors (DBR) and PhC cavities through band folding [8, 9] have been proposed to overcome these problems. However the bandwidth of the ultra-slow leaky mode for all these applications is limited in a narrow range, and the group velocity dispersion (GVD) shows quick variation near the slow points. Rather than obtaining a unique slow point, flat band slow light with a large bandwidth can improve the efficiency of the slow mode excitation and emission. Furthermore, except for the emission bandwidth, the directivity for some nano-antenna applications

Received 21 October 2014, Accepted 17 November 2014, Scheduled 17 November 2014

* Corresponding author: Yaocheng Shi (ycshi@coer.zju.edu.cn).

[1] Centre for Optical and Electromagnetic Research, JORCEP [Sino-Swedish Joint Research Center of Photonics], Zhejiang Provincial Key Laboratory for Sensing Technologies, Zhejiang University, East Building No. 5, Zijingang Campus, Hangzhou 310058, China.

[2] ZJU-SCNU Joint Research Center of Photonics, Centre for Optical and Electromagnetic Research, South China Academy of Advanced Optoelectronics, South China Normal University (SCNU), Guangzhou 510006, China.

on PhC waveguide is also important. Some directive antennas with high zenithal directivity have already been demonstrated on the PhC [10–13], but without much consideration on the efficiency and bandwidth.

Among these structures mentioned above, a leaky mode mechanism based on coupled-mode theory and flat-band slow light is useful [14]. Distinguished performance for the flat-band slow mode in the leaky region is preferred for cavity-free lasing and antenna-like directive emission applications.

Line-defect is one of the most important elements to achieve slow light [15–17]. The dispersion of the line-defect PhC waveguide can be engineered by rearrangement of the nearest-neighbour lattice [18–20]. Chirped arrangement [21] and introduction of different ring-shaped and ellipse-shaped holes [22, 23] have been demonstrated to obtain high delay-bandwidth products. In addition to the even-mode slow light realized in line-defect PhC waveguides, odd-mode slow light has also been demonstrated by using asymmetric PhC waveguides [24, 25]. Even if a high delay-bandwidth product can be obtained [26, 27], the dispersion outside the guided region has not yet been investigated.

In this paper, we propose a novel, modified line-defect PhC waveguide by introducing metal strips beside the air holes to engineer the dispersion of the odd mode in the leaky mode region. The band engineering of the proposed device is investigated by using the three-dimensional finite difference time domain (3D-FDTD) method. The position of the metal strip can be tuned to achieve a linear band in the photonic band structure and a flattened stop-like shape in the group index curve. An optimized hybrid photonic crystal (HPhC) waveguide with a nearly-constant average group index of 192 and 2 nm (i.e., 330 GHz) bandwidth has been demonstrated with no obvious waveform distortion.

2. DESIGN AND ANALYSIS

The group velocity ν_g of light with frequency ω in the PhC waveguide is given as:

$$\nu_g = \frac{d\omega}{dk} = \frac{c_0}{n_g}, \tag{1}$$

where k is the wavevector along the waveguide, n_g is the group index and c_0 is the light velocity in vacuum. In addition to the first order dispersion (v_g), the second order dispersion — GVD is also calculated as follow:

$$\beta_2 = \frac{d^2k}{d\omega^2} = \frac{dn_g}{d\omega}\frac{1}{c_0}. \tag{2}$$

The normalized delay-bandwidth product (NDBP) is used to evaluate the performance for slow light:

$$\text{NDBP} = \langle N_g \rangle \cdot (\Delta\omega/\omega_0), \tag{3}$$

where N_g and $\Delta\omega$ is the group index and bandwidth for the average slow region and ω_0 the central frequency of the slow band.

Figure 1(a) shows the schematic diagram of the proposed HPhC waveguide, and the inset on the left-bottom corner shows the cross section. The waveguide consists of two rows of air holes on each side

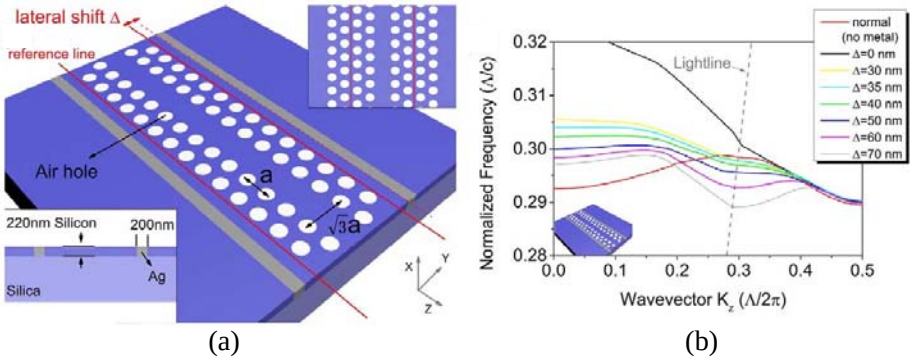

(a) (b)

Figure 1. (a) Schematic of the proposed HPhC waveguide. The cross section of the structure is shown in the lower left inset. (b) Dispersion curves for the HPhC waveguides with varying lateral shift Δ.

with Ag strips. A silicon-on-insulator (SOI) platform with a 220 nm thick silicon layer is considered in our work. In the following analysis, the refractive index of the Si layer and the silica insulator layer are chosen to be 3.45 and 1.455 respectively. The complex permittivity of Ag is obtained from the experimental data of Johnson and Christy [28]. A proper set of parameters for Drude model fitting are: background dielectric constant $\varepsilon_\infty = 5$, plasma frequency $\omega_p = 1.38 \times 10^{16}$ rad/s, and collision frequency $\gamma = 5.07 \times 10^{13}$ rad/s [29]. The period and the radius for the air holes are chosen to be $\Lambda = 410$ nm and $r = 126$ nm, respectively. A "reference line", depicted by red solid line, is introduced to determine the position of the Ag strips. The reference line is the symmetric axis for the second and the third row of air holes in the standard PhC waveguide (inset at the upper right corner). The position for the Ag strips can be described by the lateral shift "Δ" away from the waveguide.

As plane wave expansion (PWE) is inapplicable for solving the metal problem, the 3D FDTD method is used for the band diagram simulation. Figure 1(b) shows the dispersion curves for different Δ. The red line, which dramatically steepens when being away from the zero point and Bloch points, depicts the dispersion of the normal PhC waveguide. We found that the dispersion curves are strongly influenced by the position of the Ag strips, e.g., different Δ. We can see that, when $\Delta = 0$ nm, the dispersion slopes and rises to a very high frequency and begins dropping for $\Delta \geq 0$ nm. Thus, we can tune the dispersion by changing the Δ. From Figure 1(b), we can also find that when $\Delta = 30$–50 nm, the dispersion curves can be flattened and become monotonous. The leaky region where the normalized wave vector along the waveguide $k_x = 0$–0.155 is much flatter than the others.

While the slow delay and bandwidth are always coupled tradeoffs, larger group delay means narrowed bandwidth. We then use Eq. (1) to calculate the group index for the situation $\Delta = 35$, 40, 50 and 60 nm. From Figure 1(b) we can see that the HPhC waveguide with $\Delta = 35$ nm has the most flat dispersion in the leaky mode region, while the one with $\Delta = 60$ nm has the larger bandwidth. The group index for the HPhC waveguide with lateral shift $\Delta = 40$ and 50 nm is shown in Figure 2(a). The calculated results show that the HPhC waveguide with $\Delta = 50$ has lower group indices and larger bandwidth compared to the one of $\Delta = 40$. Although the maximum group index existing at the boundary of the slow region for $\Delta = 50$ nm can reach a value up to 10^4, the effective flat region is concentrated where the group index is lower than 250. The calculated average region is within 10% around the average group index [14, 19]. Group index in this region is calculated and an average value of 192 is obtained, while the normalized bandwidth $\Delta\omega/\omega$ decreases to 0.0015. A NDBP of 0.288 is also obtained. For $\Delta = 40$ nm, the average group index, normalized bandwidth $\Delta\omega/\omega$ and NDBP are calculated to be 368, 0.0007 and 0.258, respectively. For $\Delta = 60$ nm (not shown in Figure 2), the average group index is calculated to be 153 with a 0.0017 normalized bandwidth, and a NDBP of 0.255 is also obtained. Among these calculated values, the largest one for NDBP is obtained at $\Delta = 50$ nm. Numerically, bandwidth and group index in the flat band region ($\Delta = 35$–50 nm) will balance each other out when Δ varies in this flat band region ($\Delta = 35$–50 nm), and the corresponding NDBP (calculated by Eq. (3)) of this waveguide remains nearly constant around 0.275. As the shift Δ further decreases, the bandwidth is tremendously constricted to a small value but with a much larger group index that

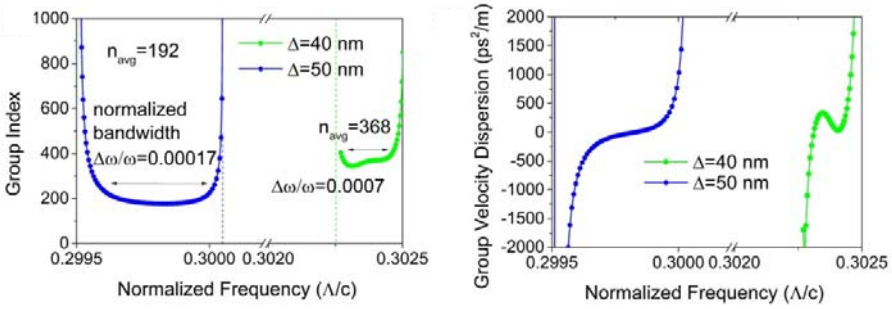

Figure 2. Group index (a) calculated by Eq. (1) and group velocity dispersion (b) calculated by Eq. (2) in the leaky mode slow light region.

exceeds 10^5, especially when $\Delta = 35\,\text{nm}$. The slow band is then compressed to a "stopped point" (not shown in Figure 2), which is excellent for nanolasing and for single photonic sources [3–7]. The GVD calculated by Eq. (2) is presented in Figure 2(b). From the figure, we can find that these two regions mentioned above exhibit very-low GVD. The highest peaks of GVD concentrate on the rising and falling edge of the group index and make no difference on the "average" ultra-slow bands. However, due to the step-shape group index for $\Delta = 40\,\text{nm}$, the GVD exhibits a twist.

According to the above analysis, this HPhC waveguide conserves the characteristics of the flat-band while balancing the delay and bandwidth. For $\Delta = 50\,\text{nm}$, a relatively large group index and bandwidth can be obtained simultaneously, which is attractive for applications involving light harvesting and directive emission. When an ultra-slow position is optimized, the bandwidth can be compressed to a nearly monochromatic "stopped" point (within $\Delta = 30$–$40\,\text{nm}$, near $\Delta = 35\,\text{nm}$) with an ultra-large group index, which may be used for cavity-free nanolasing with a large Purcell factor. Thus, flexible applications can be achieved by choosing different values for lateral shift Δ.

3. SLOW-LIGHT VERIFICATION IN THE TIME DOMAIN AND FAR-FIELD CHARACTERISTIC

Time-domain pulse propagation simulation was performed to verify the slow light properties in the HPhC waveguides (Figure 3(a)). A Gaussian pulse with FWHM of 200 fs is launched in asymmetric position to the HPhC waveguide in order to excite the odd mode, while 2 monitors with a distance of Λ in the center of the waveguide are used to record the transmitted power. The working point is chosen at $(k_x, f) = (0.1, 0.299984c/\Lambda)$. As the mode is leaky, an observation plane with an area covering the whole simulation region is placed 400 nm above the waveguide to collect the leaky mode coupling to the free space. As shown in Figure 3(b), the slow mode arrives at Monitor 1 at 422 fs and Monitor 2 at 710 fs; thus a group index of 211 is obtained, which is consistent with the value obtained from the dispersion calculations. Furthermore, we can find that there is not much distortion of the pulse shape (2.5% pulse broadening in FWHM) in these two positions. The amplitude decreases tremendously because of the leaky coupling.

The time-averaged power distribution of $|E|^2$ and the far-field pattern for the optimized HPhC waveguide with $\Delta = 50\,\text{nm}$ are depicted in Figures 4(a) and (c), respectively. For purposes of comparison, the corresponding power distribution and far-field pattern from the normal PhC waveguide are also given in Figures 4(d) and (f). The corresponding distribution of electric field E_y has been shown in Figures 4(b) and (e), respectively. We can find that the field is tightly confined in the nearest two rows of holes for the normal PhC waveguide, while the field is mainly confined in the line defect, and part of them is distributed near the metal strip. It is the slight lateral shift Δ that pushes the field close to the vicinity of the metal and helps to slow down the leaky mode. The collected power from the HPhC waveguide to the free space (calculated at observation plane) can be up to 40% of the source. As the light will couple upward and downward, the coupling exhibits a very high efficiency. As shown in Figure 1(a), the width of the strip is chosen to be 200 nm, which is larger than the skin depth of

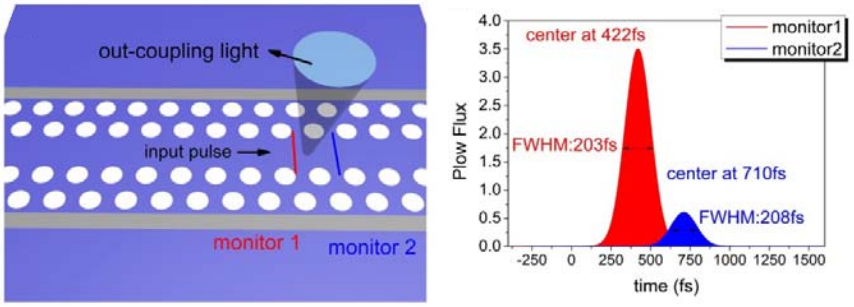

(a) (b)

Figure 3. (a) Structure for exciting pulse and schematic diagram for interrogation. (b) The waveform is captured by the line monitor, with amplitude 1 at 0.227 μm, 60 fs and amplitude 0.19 at 1.465 μm, 829 fs. The working point is chosen at $(k_x, f) = (0.1, 0.299984c/\Lambda)$.

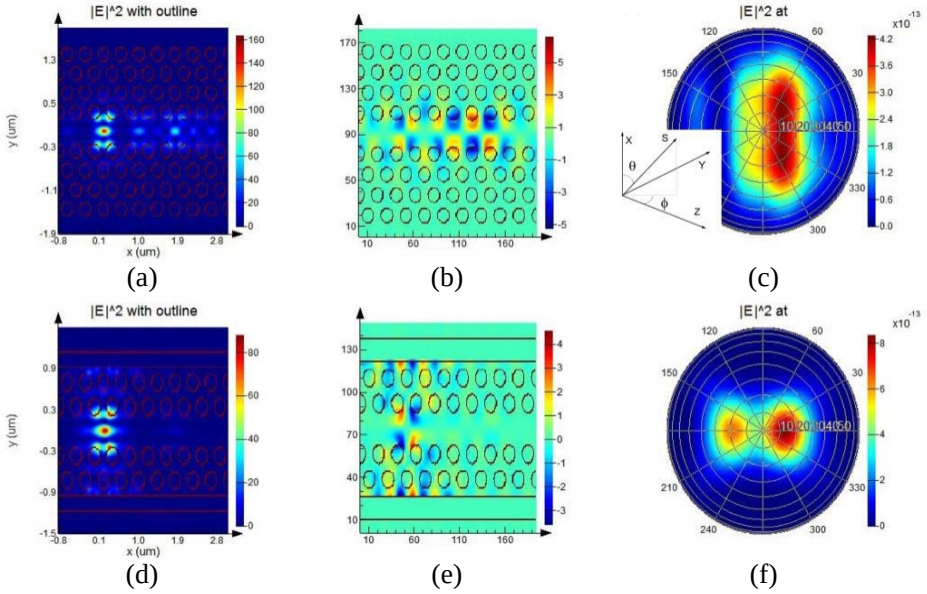

Figure 4. (a) & (d) Time-averaged power distribution of $|E|^2$ in normal and HPhC waveguides, respectively. (b) & (e) The corresponding electric field E_y. (c) & (f) The corresponding far-field pattern obtained at the observation plane.

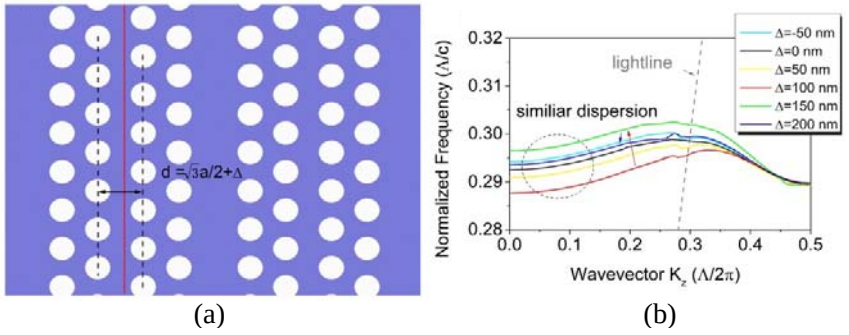

Figure 5. (a) Schematic diagram of the normal PhC waveguide with partial lateral shift Δ. The lateral shift occurs at the gap between the first and the second row of air hole. (b) The corresponding dispersion for PhC waveguides with different Δ. All the sweep parameters are labeled in the legend. The rising and falling behaviors are depicted by the red and blue arrows, respectively. The turning point for the dispersion is at $\Delta = 150\,\text{nm}$.

the frequency band we used, and thus a better confinement of light is formed in the HPhC waveguide compared to the normal one. The far-field patterns are given in Figures 4(c) and (f). We can observe that the coupling angle θ for both structures along the propagating direction is near 17°, consistent with the calculated value of 18.9° according to Snell's Law. Moreover, we should note that the large azimuthal angle of the normal PhC waveguide's original far-field pattern is compressed from a value of up to $|\varphi| > 60°$ to a very small one ($|\varphi| < 30°$) with fixed θ by introducing the metal strips. This can be explained by the incomplete lattice broken by the metal. With such a concentrated coupling angle, the exciting of the slow mode and the collection of out-coupling light can be much easier.

4. CONTRIBUTION OF SYMMETRIC ARRANGEMENT TO FLAT DISPERSION

We try to understand the working principle for the proposed structure. The Ag metal strip can be treated as a reflective mirror. Thus, we first analyze the normal PhC waveguide with the mirrored hole

arrangement. The schematic diagram is depicted by Figure 5(a). Lateral shift Δ has been introduced to the mirrored air holes to engineer the dispersion. The normal distance between the second and third row of air holes is $d = d_0 + \Delta$ ($d_0 = \mathrm{sqrt}(3)\Lambda/2$). Figure 5(b) shows the calculated dispersion curves for the PhC waveguide with mirrored air holes. We can find that all these dispersion curves exhibit similar slopes. Flat-band slow light cannot be found in the leaky mode region.

The time-averaged power distribution of $|E|^2$ in the PhC waveguide with lateral shift $\Delta = 150\,\mathrm{nm}$ is shown in Figure 6(a). The working point is chosen at $(k_x,\ f) = (0.1,\ 0.276258c/\Lambda)$. From Figure 6(a) we can see that, due to the lateral shift, a small fraction of light is funnelled into the gap between the 2nd and 3rd row of holes while the rest is still confined in the line defect waveguide. The corresponding electric field E_y in Figure 6(b) exhibits asymmetric-like patterns, which result in unstable light transmission and weaker confinement for light. The far-field pattern for this waveguide is also shown in Figure 6(c). When the normalized wave vector is fixed at 0.1, the coupling angle θ along the waveguide is around 15°–25°. Compared to the normal waveguide, the emission direction is centralized more at the two branches with a large azimuthal angle of about $|\varphi| > 60°$ rather than that along the waveguide.

The introduction of the metal may result in a symmetric electric field across the metal-dielectric interface with the same polarization and phase for the electric field as that perpendicular to the interface. Similarly, we introduce a symmetrical arrangement to the normal PhC waveguide, [shown in Figure 7(a)]. The 2nd and 3rd rows of air holes are symmetric, with the axis labeled with the green line. The corresponding dispersion curves for such PhC waveguides are presented in Figure 7(b). With a changing lateral shift Δ, there is always rising and falling behavior with different turning points. The slope of the dispersion also changes with different Δ. While $\Delta = 100\,\mathrm{nm}$, the dispersion curve is flattened with a relatively high frequency. The frequency tuning effect can be controlled by the lateral shift.

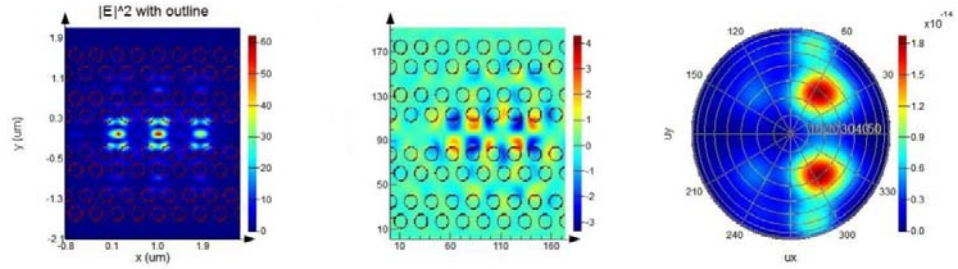

Figure 6. (a) Time-averaged power distribution of $|E|^2$ in normal waveguide with lateral shift $\Delta = 150\,\mathrm{nm}$. (b) The corresponding electric field E_y. (c) The corresponding far-field pattern calculated at the observation plane.

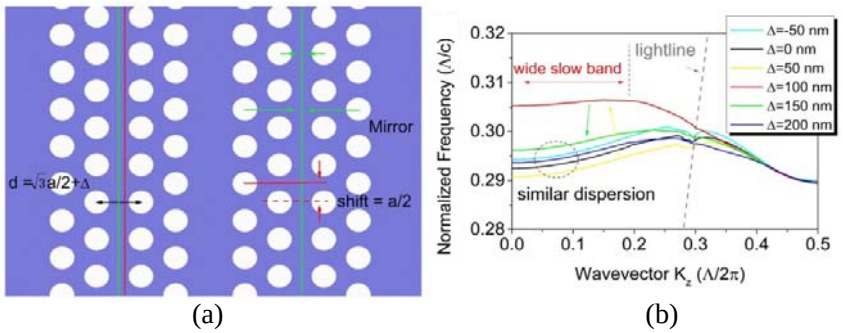

Figure 7. (a) Schematic diagram of the normal PhC waveguide with partial lateral shift Δ and extra symmetric arrangement. The lateral shift occurs at the gap between the first and second rows of air holes. The symmetric axis is labeled by the green line. (b) The corresponding dispersion for the changed Δ. All the sweep parameters are labeled in the legend. The rising and falling behaviors are indicated by the yellow and green arrows. The turning point for the dispersion is at $\Delta = 100\,\mathrm{nm}$.

For comparison, the average group index and GVD are also shown in Figure 8(a). An average group index of 89 is obtained for $\Delta = 100\,\text{nm}$ with a 0.00251 normalized bandwidth, resulting in a NDBP of 0.224, which is smaller than that of the HPhC. The GVD also exhibits a low value due to the flat construction. The far-field pattern is shown in Figure 8(b), with working point $(k_x,\ f) = (0.1,\ 0.3062510c/\Lambda)$. Similar to that of a normal PhC waveguide, the pattern also exhibits a large azimuthal angle $|\varphi| > 60°$, which accounts for the multidirectionality of PhC. The coupling power is also calculated at the observation plane, and a total efficiency of about 0.32 is obtained. Here the time-averaged power distribution of $|E|^2$ and the corresponding component E_y of the electric field in Figures 8(c) & (d) results in the flat dispersion. The electric field of the symmetric PhC waveguide leaks to the side channel created by the lateral shift, which is similar to that of the HPhC. Furthermore, the symmetric arrangement contributes to the symmetric electric field distribution [Figure 8(d)]. Since metal originally has a symmetrical effect on the electric field, which will result in a side-channel symmetric field near the metal in the HPhC waveguide, the coincidence between HPhC and symmetric

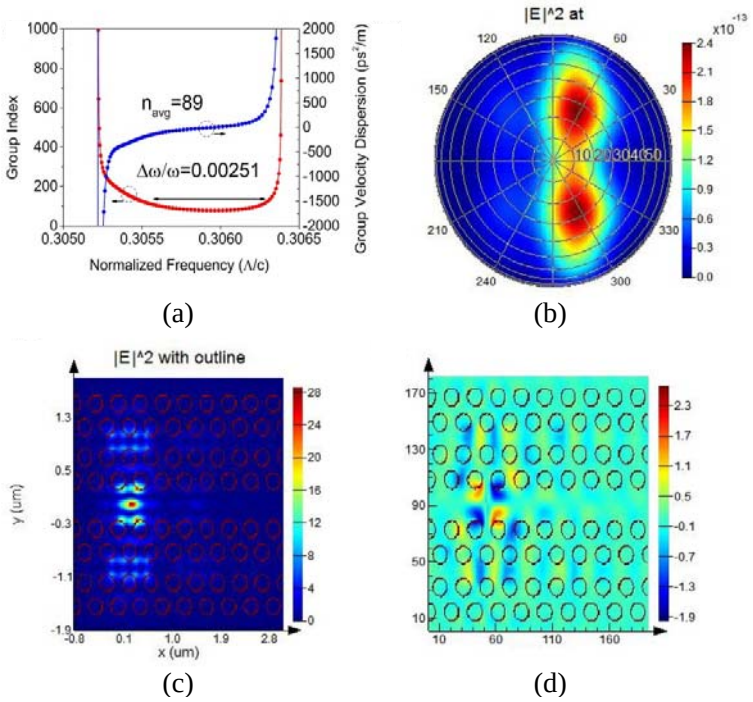

Figure 8. (a) Average group index and GVD for $\Delta = 100\,\text{nm}$. (b) The corresponding far-field pattern calculated at the observation plane. The working point is chosen at $(k_x,\ f) = (0.1,\ 0.3062510c/\Lambda)$. (c) Time-averaged power distribution of $|E|^2$ in normal and HPhC waveguide. (d) The corresponding component E_y of electric field.

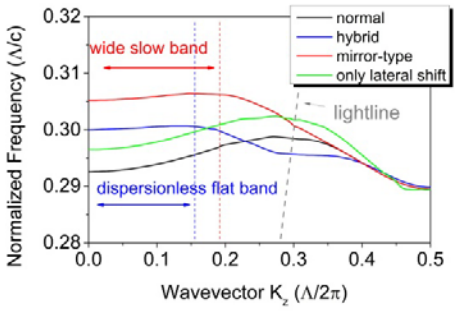

Figure 9. A comparison of dispersion curves for normal, hybrid, lateral-shifted and symmetrical PhC waveguides.

waveguides, shown in Figure 4(e) and Figure 8(d), results in the flat dispersion that results from symmetric field distribution in the side channels. However, due to the decentralization of power in this symmetric waveguide, more rows of holes are needed at each side of the waveguide to maintain a similar confinement for light, which enlarges the whole size. The lower out-coupling efficiency also attributes to this decentralization.

In summary, we have demonstrated an HPhC waveguide featuring flexible ultra-flat-band slow light and explained the mechanism for flattening the dispersion by discussing the effect of the symmetrical arrangement. A comparison of the dispersion curves for different PhC waveguides is shown in Figure 9. Although both the symmetric PhC waveguides and HPhC waveguides can engineer the dispersion to achieve slow light, the HPhC waveguides exhibit a higher NDBP, much small azimuthal angle and high out-coupling efficiency, which are more attractive for out-coupling applications.

5. CONCLUSION

In summary, we have presented a new kind of HPhC waveguide for slow light with ultra-flat dispersion. The introduction of the metal strip and the lateral shift can engineer the dispersion of the slow mode in the leaky mode region and offers flexibility for different flat-band applications. A normalized bandwidth of 0.0015 with an average group index of 192 and thus a NDBP of 0.288 can be obtained in the leaky mode region. Ultra high group index (nearly "stopped light") at a certain frequency can also be obtained by tuning the lateral shift Δ. A comparison between different types of PhC waveguides explains the working principle of the flat dispersion. The HPhC waveguides with high group index, low dispersion, flexible flat-band tuning, high coupling efficiency, small azimuthal angle and small package are favorable for cavity-free optical devices, threshold-free nanolasing and other applications based on directive emission. Optical soliton which profits from choreographed GVD is also under research.

ACKNOWLEDGMENT

This work is supported by the National High Technology Research and Development Program (863) of China (No. 2012AA012201), the National Natural Science Foundation of China (Grant Nos. 61377023, 91233208 and 61108022), the Guangdong Innovative Research Team Program (Grant No. 201001D0104799318), and the Zhejiang Provincial Natural Science Foundation of China (Grant No. LY13F050002). We thank Prof. Daoxin Dai, Prof. Liu Liu, Xiaochen Ge, Shoubao Han, Qiangsheng Huang for valuable discussions.

REFERENCES

1. Hess, O., J. Pendry, S. A. Maier, R. F. Oulton, J. M. Hamm, and K. L. Taskmakidis, "Active nanoplasmonic metamaterials," *Nat. Mat.*, Vol. 11, 573–584, 2012.
2. Taskmakidis, K. L., A. D. Boardman, and O. Hess, "'Trapped' rainbow storage of light in metamaterials," *Nature*, Vol. 450, 397–401, 2007.
3. Taskmakidis, K. L., T. W. Pickering, J. M. Hamm, A. F. Page, and O. Hess, "Completely stopped and dispersionless light in plasmonic waveguides," *Phys. Rev. Lett.*, Vol. 112, 167401(1)–167401(5), 2013.
4. Pickering, T., J. M. Hamm, J. F. Page, S. Wuestner, and O. Hess, "Cavity-free plasmonic nanolasing enabled by dispersionless stopped light," *Nat Comm.*, Vol. 5, 4972, 2014.
5. Rao, V. S. C. M. and S. Hughes, "Single quantum-dot Purcell factor and Beta factor in a photonic crystal waveguide," *Phys. Rev. B*, Vol. 75, 205437, 2007.
6. Yao, P., C. V. Vlack, A. Reza, M. Petterson, M. M. Dignam, and S. Hughes, "Ultrahigh Purcell factors and Lamb shifts in slow-light metamaterial waveguides," *Phys. Rev. B*, Vol. 80, 195106, 2009.
7. Ek, S., E. Semenova, P. Lunnemann, K. Yvind, and J. Mork, "Enhanced gain in photonic crystal amplifiers," *IEEE ICTON*, 1–4, 2012.

8. Tran, N. V. Q., S. Combrie, and A. D. Rossi, "Directive emission from high-Q photonic crystal cavities through band folding," *Phys. Rev. B*, Vol. 79, 041101, 2009.
9. Benyatto, T., E. Gerelli, L. Milord, C. Jamois, A. Harouri, C. Chevalier, C. Seassal, A. Belarouci, X. Letartre, and P. Viktorovitch, "Slow Bloch mode cavity for optical trapping," *IEEE ICTON*, 1–5, 2013.
10. Brown, E. R. and O. B. McMabon, "High zenithal directivity from a dipole antenna on a photonic crystal," *Appl. Phys. Lett.*, Vol. 68, 1300–1302, 1996.
11. Temelkuran, B., M. Bayindir, E. ozbay, R. Riswas, M. M. Sigalas, G. Tuttle, and K. M. Ho, "Photonic crystal-based resonant antenna with a very high directivity," *Appl. Phys. Lett.*, Vol. 87, 602–605, 2000.
12. Tevenot, M., C. Cheype, A. Reineix, and B. Jecko, "Directive photonic-bandgap antennas," *IEEE Trans. on Micr. Theo. and Tech.*, Vol. 47, 2115–2122, 1999.
13. Sa, Z. H., Y. Poo, R. X. Wu, and C. Xiao, "An implementation of directional antenna by self-biased magnetic photonic crystal," *Appl. Phys. A*, Vol. 117, No. 2, 427–431, Springer, 2014.
14. Hu, J. and C. R. Menyuk, "Understanding leaky modes: Slab waveguide revisited," *Advs. in Optics and Photon.*, Vol. 1, 58–106, 2009.
15. Baba, T. and D. Mori, "Slow light engineering in photonic crystal," *J. Phys. D: Appl. Phys.*, Vol. 40, 2659–2665, 2007.
16. Krauss, T. F., "Slow light in photonic crystal waveguides," *J. Phys. D: Appl. Phys.*, Vol. 40, 2666–2670, 2008.
17. Liang, J., L. Ren, M. Yun, X. Han, and X. Wang, "Wideband ultraflat slow light with large group index in a W1 photonic crystal waveguide," *Appl. Phys. Lett.*, Vol. 110, 063103, 2011.
18. Frandsen, L. H., A. V. Lavrinenko, J. Fage-Pedersen, and P. I. Borel, "Photonic crystal waveguides with semi-low light and tailored dispersion properties," *Opt. Express*, Vol. 14, 9444–9450, 2006.
19. Mann, N., S. Combrie, M. Patterson, A. D. Rossi, and S. Hughes, "Reducing disorder-induced losses for slow light photonic crystal waveguides through Bloch mode engineering," *Opt. Lett.*, Vol. 38, 4244–4247, 2013.
20. How, J., D. Gao, H. Wu, R. Hao, and Z. Zhou, "Flat band slow light in symmetric line defect photonic crystal waveguides," *IEEE Photon. Tech. Lett.*, Vol. 21, 1571–1573, 2009.
21. Baba, T., T. Kawasaki, H. Sasaki, J. Adachi, and D. Mori, "Large delay-bandwidth product and tuning of slow light pulse in photonic crystal coupled waveguide," *Opt. Express*, Vol. 16, 9245–9253, 2008.
22. Xu, Y., L. Xiang, E. Cassan, D. Gao, and X. Zhang, "Slow light in an alternative row of ellipse-hole photonic crystal waveguide," *Appl. Opt.*, Vol. 52, 1155–1160, 2013.
23. Saynatjoki, A., M. Mulot, J. Ahopelto, and H. Lipsanen, "Dispersion engineering of photonic crystal waveguides with ring-shaped holes," *Opt. Express*, Vol. 15, 8323–8328, 2007.
24. Ma, J. and C. Jiang, "Demonstration of ultraslow modes in asymmetric line-defect photonic crystal waveguides," *IEEE Photon. Tech. Lett.*, Vol. 20, No. 14, 1237–1239, 2008.
25. Ma, J. and C. Jiang, "Flatband slow light in asymmetric line-defect photonic crystal waveguide featuring low group velocity and dispersion," *IEEE Journal of Quant. Electron.*, Vol. 44, No. 8, 763–769, 2008.
26. Hao, R., E. Cassan, H. Kurt, X. L. Roux, D. Marris-Morini, L. Vivien, H. Wu, Z. Zhou, and X. Zhang, "Novel slow light waveguide with controllable delay-bandwidth product and ultra-low dispersion," *Opt. Express*, Vol. 18, 5942–5950, 2010.
27. Hao, R., E. Cassan, X. L. Roux, D. Gao, V. D. Khanh, L. Vivien, H. D. Marris-Morini, and X. Zhang, "Improvement of delay-bandwidth product in photonic crystal slow-light waveguides," *Opt. Express*, Vol. 18, 16309–16319, 2010.
28. Johnson, P. and R. Christy, "Optical constants of noble metals," *Phys. Rev. B*, Vol. 6, 4370–4379, 1972.
29. Palik, E. D., *Handbook of Optical Constants of Solids,* Academic Press, 1998.